Supplementary Information

Controlling Crystallization Dynamics of Sn-Pb Mixed Perovskite Films for Efficient Scalable Photovoltaics

Ting Pan[a], Tonghan Zhao[b], Roja Singh[ab], Felix Laufer[ab], Weimu Xu[a], Julian Petermann[ab], Benjamin Hacene[a], Alexander Diercks[a], Thomas Feeney[ab], Sachin Kinge[c], Lingyi Fang[ab], Hang Hu[*ab], Ulrich Wilhelm Paetzold[*ab]

[a] Light Technology Institute (LTI), Karlsruhe Institute of Technology (KIT), Engesserstrasse 13, 76131 Karlsruhe, Germany

[b] Institute of Microstructure Technology (IMT), Karlsruhe Institute of Technology (KIT), Hermann-von-Helmholtz-Platz 1, 76344 Eggenstein-Leopoldshafen, Germany

[c] Materials Engineering Department, R&D 2, Toyota Motor Europe, 1930 Zaventem, Belgium

[*]Corresponding authors: hang.hu@kit.edu (H.H.), ulrich.paetzold@kit.edu (U.W.P.)

Experimental Section

Materials

Methylammonium iodide (MAI, GreatCell, 99.9%), formamidinium iodide (FAI, GreatCell, 99.9%), cesium iodide (CsI, Alfa Aesar, 99.9%), lead iodide (PbI_2, Alfa Aesar, 99.99%), lead bromide ($PbBr_2$, Alfa Aesar, 99.99%), tin iodide (SnI_2, Sigma-Aldrich, 99.999%), lead thiocyanate ($Pb(SCN)_2$, Sigma-Aldrich, 99.5%), tin fluoride (SnF_2, Sigma-Aldrich, 99%), methylammonium chloride (MACl, GreatCell, 99.99%), dimethylformamide (DMF, Sigma-Aldrich, anhydrous, 99.8%), dimethyl sulfoxide (DMSO, Sigma-Aldrich, anhydrous, 99.9%), 1,2-dichlorobenzene (DCB, Sigma Aldrich, anhydrous, 99%), Poly(3,4-ethylenedioxythiophene) polystyrene sulfonate (Clevios™ P VP AI 4083 PEDOT:PSS, 1.3-1.7 wt.%), ethane-1,2-diammonium iodide ($EDAI_2$, Sigma Aldrich, anhydrous, 98%), 4-fluoro-phenethylammonium chloride (4F-PEACl, Greatcell Solar Materials, 99%), phenyl-C61-butyric acid methyl ester (PCBM, Sigma Aldrich, 99%), fullerene (C_{60}, Sigma Aldrich, 99.5%), 2,9-dimethyl-4,7 diphenyl-1,10-phenanthroline (BCP, Luminescence Technology, 99%), silver (Ag), ITO-coated glass substrates (120 nm, sheet resistance 15 Ω sq^{-1}, Luminescence Technology).

Preparation of narrow-bandgap (NBG) perovskite precursor

A 2.0 M $Cs_{0.025}(FA_{0.8}MA_{0.2})_{0.975}Sn_{0.5}Pb_{0.5}I_3$ perovskite precursor was prepared by dissolving 1.0 M SnI_2, 1.0 M PbI_2, 1.56 M FAI, 0.39 M MAI, 0.05 M CsI, 0.01

M $Pb(SCN)_2$, and 0.05 M SnF_2 in a solvent mixture of DMF and DMSO (volume ratio of 6.5:1). The precursor was then stirred overnight and filtered with a 0.2 μm PTFE filter before use. 0.75%, 1.5%, 3%, 6%, and 10% MACl precursors were prepared by dissolving excess 0.015, 0.03, 0.06, 0.12, and 0.2 M MACl in the filtered reference precursor, respectively. All precursors were prepared in a N_2 glovebox (O_2 < 1.0 ppm and H_2O < 0.4 ppm). The above solution was used for spin-coating. For blade-coating, the precursor was diluted to 1.0 M using a DMF:DMSO (6.5:1) solvent mixture.

Preparation of wide-bandgap (WBG) perovskite precursor

A 1.4 M $Cs_{0.2}FA_{0.8}Pb(Br_{0.4}I_{0.6})_3$ WBG perovskite precursor was prepared by dissolving 0.28 M CsI, 1.12 M FAI, 0.56 M PbI_2, and 0.84 M $PbBr_2$ in a solvent mixture of DMF and DMSO (volume ratio of 4:1). The precursor was then stirred overnight and filtered with a 0.2 μm PTFE filter before use.

Fabrication of NBG perovskite solar cells

The NBG PSCs were fabricated in a planar architecture with the stack of glass / ITO / PEDOT:PSS / $Cs_{0.025}(FA_{0.8}MA_{0.2})_{0.975}Sn_{0.5}Pb_{0.5}I_3$ / $EDAI_2$ / PCBM / C_{60} / BCP / Ag. The ITO substrates were cleaned ultrasonically with deionized water, acetone, and isopropanol, sequentially, for 10 min each. Before use, the substrates were treated by O_2 plasma for 5 min. 65 μL of diluted PEDOT:PSS solution (PEDOT:PSS/IPA = 1:3 volume ratio) was deposited on cleaned ITO substrates

by spin coating at 5500 rpm for 30 s, followed by annealing at 140 ℃ for 10 min. The prepared PEDOT: PSS-coated substrates were transferred to a N_2-filled glovebox immediately. The perovskite wet films were fabricated by either spin-coating or blade-coating methods. In the spin-coating method, 50 μL of the 2 M precursor was dropped onto the 16 mm × 16 mm^2 PEDOT:PSS-coated substrates and spin-coated at 6000 rpm for 10 s with a ramp rate of 2000 rpm s^{-1}. In the blade-coating method, 30 μL of 1 M precursor was dropped onto the 32 mm × 64 mm^2 PEDOT:PSS-coated substrates and then blade-coated with a coating speed of 15 mm s^{-1} and a gap height of 100 μm. The wet films were promptly transferred into a vacuum chamber and kept for 15 s for preliminary solvent extraction, which is termed vacuum quenching. For blade-coated films, the vacuum quenching (20 s) was assisted with an optimized N_2 flow to accelerate the removal of solvents. After vacuum quenching, the perovskite films were annealed at 100 ℃ for 7 min unless otherwise specified. Next, 50 μL of $EDAI_2$ (0.1 mg ml^{-1} in IPA) and PCBM (5 mg ml^{-1} in DCB) solutions were sequentially deposited on the perovskite films at 4000 rpm for 30 s (ramp rate of 2000 rpm s^{-1}) and annealed at 100°C for 5min as surface passivation. Finally, for the electron transport layers (ETLs), 30 nm C_{60}, 5 nm BCP, and 100 nm Ag were deposited sequentially by thermal evaporation. The active area of the devices was 0.105 cm^2. The champion cells were thermally evaporated with a 125-nm MgF_2 antireflection coating on the glass side of the devices. The whole process of perovskite deposition was conducted in a N_2 glovebox (O_2 < 0.2 ppm and H_2O < 0.4 ppm).

Fabrication of all-perovskite tandem solar cells

The ITO substrates were cleaned ultrasonically with deionized water, acetone, and isopropanol, sequentially, for 10 min each. Before use, the substrates were treated by O_2 plasma for 5 min. For the hole transport layers (HTLs), NiO_x nanoparticles (5 mg ml^{-1}) were firstly spin-coated at 3000 rpm for 30s and then annealed at 140 ℃ for 10 min. After cooling, Me-4PACz solution (0.4 mg ml^{-1} in methanol) was spin-coated on the NiO_x film at 4000 rpm for 30 s and then annealed at 100 ℃ for 10 min. The WBG perovskite precursor solution was spin-coated onto the HTLs at 6000 rpm for 10 s with a ramp rate of 2000 rpm s^{-1}. The wet film was then transferred into a vacuum chamber promptly and kept for 20 s to extract the preliminary solvent. After that, the sample was annealed at 100 ℃ for 10 min. Solutions of 1.0 mg ml^{-1} $EDAI_2$ and 1.0 mg ml^{-1} 4F-PEACl were spin-coated on the perovskite film sequentially at 4000 rpm for 30 s and annealed at 100°C for 5min. For the ETLs, 15 nm C_{60} was deposited by thermal deposition and 20 nm SnO_x was deposited by atomic layer deposition (ALD) with a substrate temperature of 90 ℃. Tetrakis(dimethylamino)tin (IV) (TDMASn) was used as the precursor source at that was preheated 70 °C, while H_2O source was kept in the room temperature. 15 nm indium tin oxide (ITO) was deposited by sputtering as the recombination layer. The depositions of PEDOT: PSS, NBG, C_{60}, BCP and Ag layers followed the same procedures used for the single-junction devices.

Finally, 125 nm magnesium fluoride (MgF_2) was evaporated on the glass side as an anti-reflective coating for better light management.

Current-Density–Voltage (*J–V*) Measurements

J–V curves of the devices were measured by a solar simulator (Newport Oriel Sol3A) equipped with a source meter (Keithley 2400) and a xenon lamp based on AM 1.5G (100 mW cm^{-2}) irradiation. The scan rate was set to 0.6 V s^{-1} and a certified Si reference solar cell (Newport, #2446 and #1758) was used for calibration of the spectra. The stabilized power conversion efficiency was determined by tracking the maximum power point (MPP) under continuous AM 1.5G irradiation.

In-situ Photoluminescence (In-situ PL)

PL measurements were acquired on an in-house confocal setup. The perovskite films were excited by a bright blue LED with an emission peak at 470 nm. The emitted PL signal was collected with an $f = 30$ mm plano-convex lens and filtered with a 600 nm long-pass filter. An optical fiber was employed to collect the PL signal to the Ocean HDX Spectrometer (Ocean-HDX-XR, 200-1100 nm). The laptop and spectrometer were connected via Access Point Wi-Fi. The distance between the plano-convex lens and the substrate was optimized such that the PL intensity was maximized. The positions of the substrates and the lens were kept fixed for all sample measurements to ensure better comparability. The integration

time for each individual PL spectrum was 100 ms, with a 200 ms interval between successive acquisitions.

X-ray diffraction (XRD)

XRD was conducted on the samples with the stack of ITO / PEDOT:PSS / Perovskite using a Bruker D2Phaser system equipped with Cu-Kα radiation (λ = 1.5405 Å) in Bragg–Brentano configuration and a LynxEye detector.

Scanning electron microscopy (SEM)

SEM images of the perovskite films were collected using a Zeiss LEO1530 VP scanning electron microscope with an in-lens detector. SEM images were captured using 3.00 kV or 10.00 kV acceleration voltage and an aperture size of 20 μm.

Photoluminescence mapping (PL mapping)

PL mappings were acquired with a 2.1-megapixel scientific CMOS camera (Quantalux Scmos camera, Thorlabs). PL signals were filtered with an optical filter mounted on a stationary wheel of 780 nm long-pass (Edmund Optics). The perovskite films (32 × 64 mm^2) were excited using a bright blue LED with an emission peak at 470 nm.

Atomic force microscopy (AFM)

The surface topography was inspected using Nano Wizard II (JPK Instruments). The scanning area was 10 μm × 10 μm.

Dark *J–V* curves and ideality factor measurements

Dark *J–V* curves and light intensity-dependence of V_{OC} were performed using PAIOS system with a white light emitting diode (Cree XP-G). V_{OC} can be estimated by the following equation:

$$V_{oc} = n_{id}\frac{k_B T}{q}\ln\left(\frac{j_{ph}}{j_s}+1\right)$$

where n_{id} is the ideality factor, k_B is the Boltzmann constant, T is the absolute temperature, q is the electron charge, j_{ph} is the photocurrent, and j_s is the dark saturation current.

Logarithmic V_{OC} can be linear fitted by the equation:

$$\frac{\partial V_{OC}}{\partial(\ln I)} = \frac{n_{id}k_B T}{q}$$

where n_{id} is the ideality factor, k_B is the Boltzmann constant, T is the absolute temperature, q is the electron charge, and I is the light intensity. The n_{id} values are reflected in the slopes of the curves.

The maximum FF (FF_{max}) can be empirically calculated according to the following equations:

$$FF_{max} = \frac{v_{oc} - \ln(v_{oc} + 0.72)}{v_{oc} + 1}$$

$$v_{oc} = \frac{qV_{oc}}{n_{\mathrm{id}} k_B T}$$

where k_B is the Boltzmann constant, T is the absolute temperature, q is the electron charge, and n_{id} is the ideality factor. The maximum FF is estimated without considering charge transport losses.

Charge extraction (CE)

CE was performed using the PAIOS system under different illumination intensity (1−100 mW cm^{-2}) with an illumination duration of 100 us. Integrating the extraction current over time yields the extracted charge. The extracted charge carrier density n_{CE} is then calculated according to the following equation:

$$n_{\mathrm{CE}} = \frac{1}{Lq}\left(\int_0^{t_{\mathrm{e}}} j(t)d(t) - (V_{\mathrm{a}} - V_{\mathrm{e}})C_{\mathrm{geom}}\right)$$

where L is the perovskite thickness, q is the unit charge, t_e is the extraction time, $j(t)$ is the transient current density, C_{geom} is the geometric capacitance, V_a is the voltage applied prior extraction (in most cases V_{OC}), and V_e is the extraction voltage. The charge on the capacitance needs to be subtracted as only the charge carrier density inside the bulk is of interest.

Delay-time charge extraction by linearly increasing voltage (Delay-time-CELIV)

Delay-time-CELIV was conducted using the PAIOS system under the illumination intensity of 100 mW cm^{-2} with a light-pulse length of 100 us and a ramp rate of 40 V ms^{-1}. A linearly increasing voltage in reverse direction is applied to the device $V(t) = At$, where A is the ramp rate. The linearly changing voltage induces a constant displacement current density j_{disp}, which is calculated according to the following equation:

$$j_{\text{disp}} = \frac{1}{S}\frac{dV}{dt}C_{\text{geom}} = \frac{1}{S}\frac{dV}{dt}(At)\frac{S\varepsilon\varepsilon_0}{L} = \frac{A\varepsilon\varepsilon_0}{L}$$

where S is the active area of the device, C_{geom} is the geometric capacitance, ε_0 is the vacuum permittivity, ε is the relative dielectric permittivity, and L is the perovskite thickness.

Photo charge extraction by linearly increasing voltage (Photo-CELIV)

Photo-CELIV was conducted using the PAIOS system under the illumination intensity of 100 mW cm^{-2} with a light-pulse length of 100 us and a ramp rate of 40 V ms^{-1}. A linearly increasing voltage in reverse direction is applied to the device $V(t) = At$, where A is the ramp rate. When the charge carriers are extracted

from the bulk, they create a current overshoot $\Delta j = j_{max} - j_0$. The time where the current peaks (t_{max}) can be used to calculate the charge carrier mobility by:

$$\mu = \frac{2d^2}{3At_{max}^2} \frac{1}{1 + 0.36\frac{\Delta j}{j_{disp}}}$$

where μ is the charge carrier mobility, d is the active layer thickness, A is the ramp rate, t_{max} is the time where the current peaks, j_{disp} is the displacement current and Δj is the peak current minus the displacement current. The factor $1 + 0.36 \cdot \Delta j / j_{disp}$ in the formula is an empirical correction accounting for the redistribution of the electric field.

Thickness measurement

The thickness of the perovskite thin films was examined employing a Bruker Dektakt XT profilometer.

Supplemental Figures and Tables

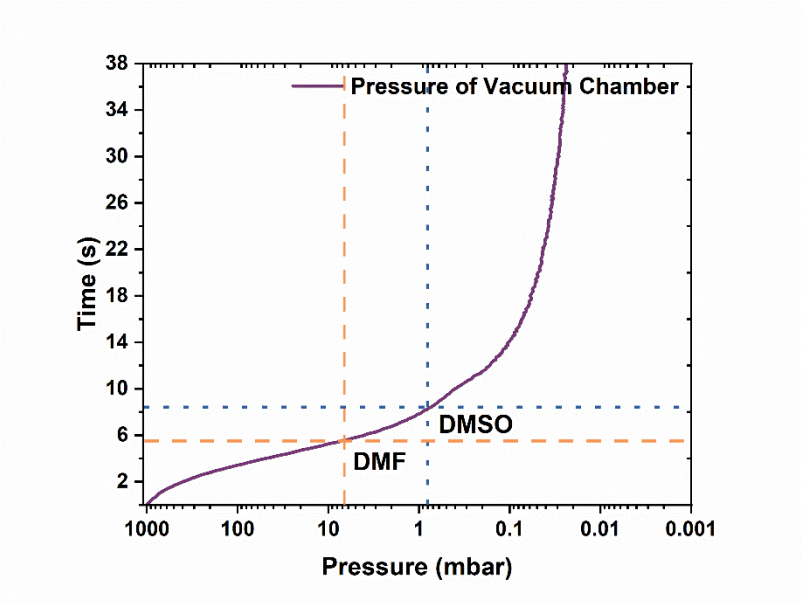

Figure S1. Pressure evolution of the vacuum chamber over time. The orange and blue dash lines represent the vapor pressure of DMF and DMSO at 25 ℃, respectively.

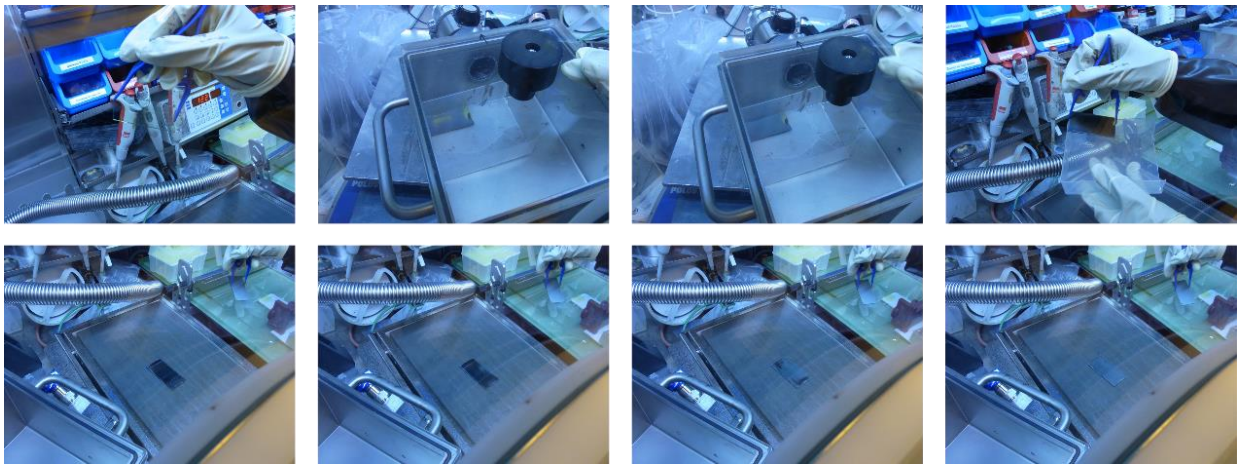

Figure S2. Photos of the evolution of perovskite formation during the vacuum quenching and annealing steps.

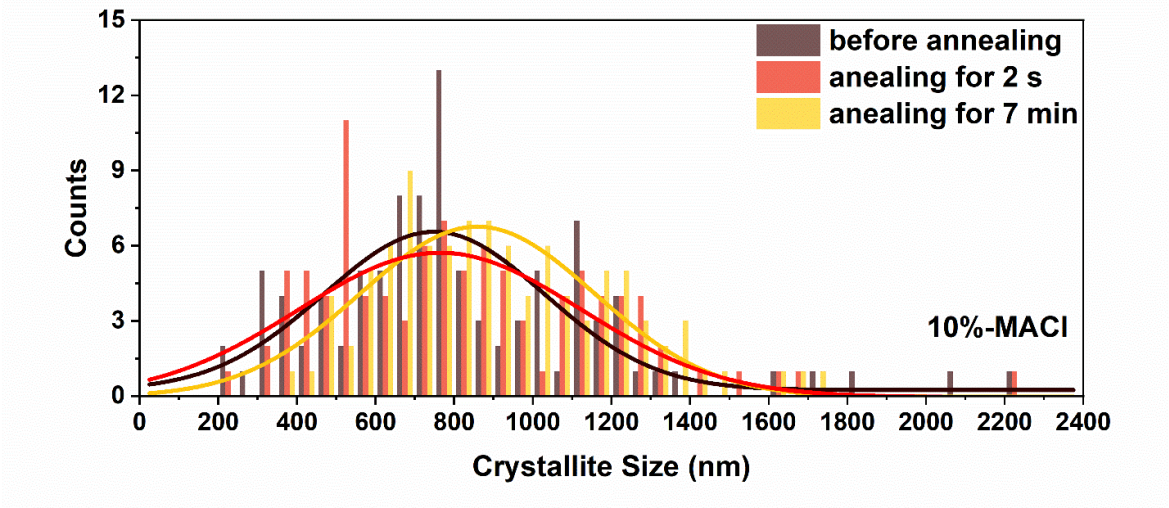

Figure S3. Grain size distribution and variation of perovskite films with 10% MACl additive before annealing (0 s), and after 2 s and 7 min of annealing.

The grain sizes are extracted from top-view SEM images using ImageJ. The grain size is determined by manually measuring the longest grain diameter using the straight-line tool in ImageJ. For each condition, 100 grains are analyzed. The grain size statistics are reported as the mean ± standard deviation. The same procedure is applied consistently to all samples.

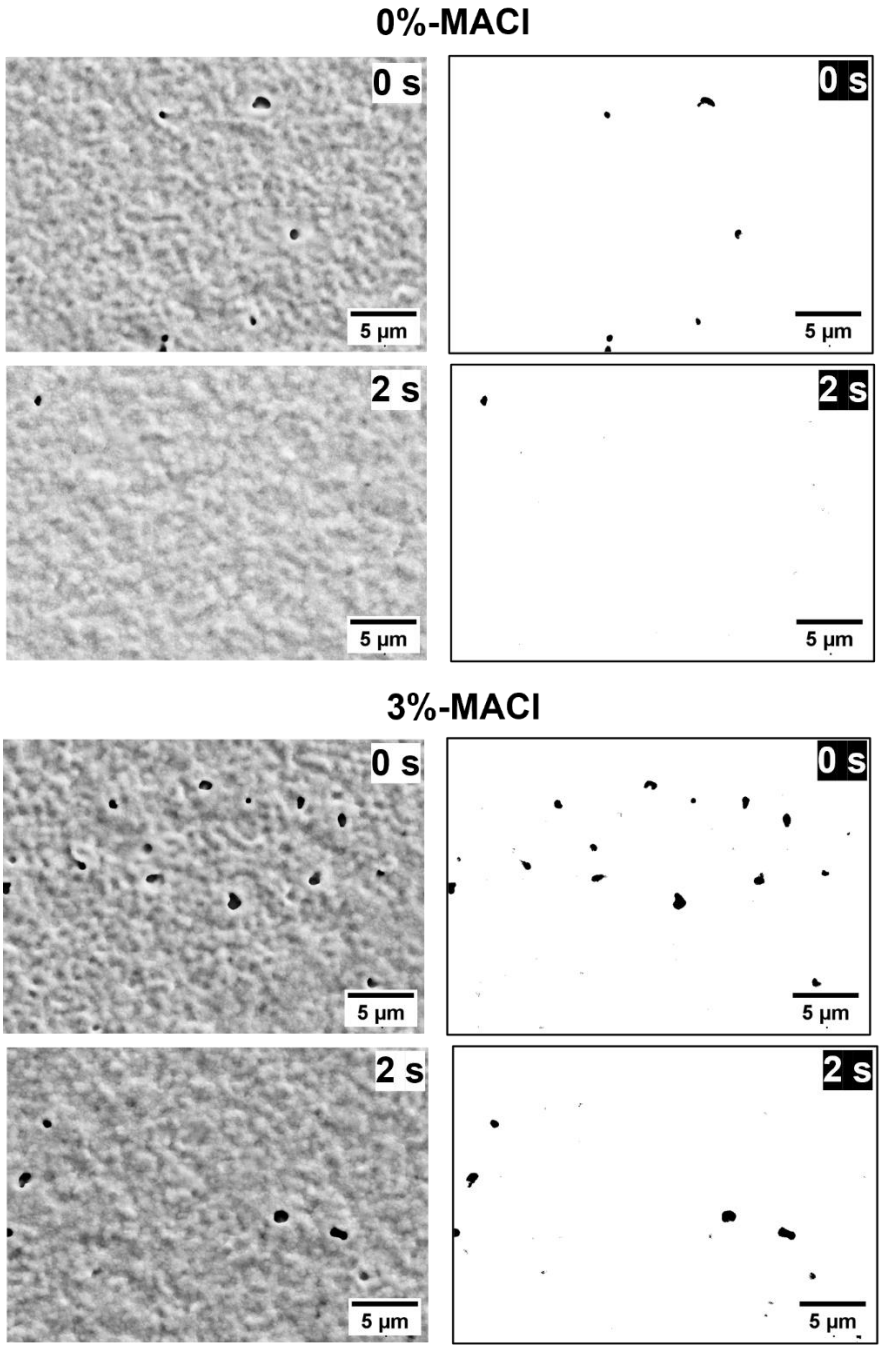

Figure S4. SEM images of pinholes before annealing (first row) and after annealing for 2 s (second row) for the perovskite films with and without MACl.

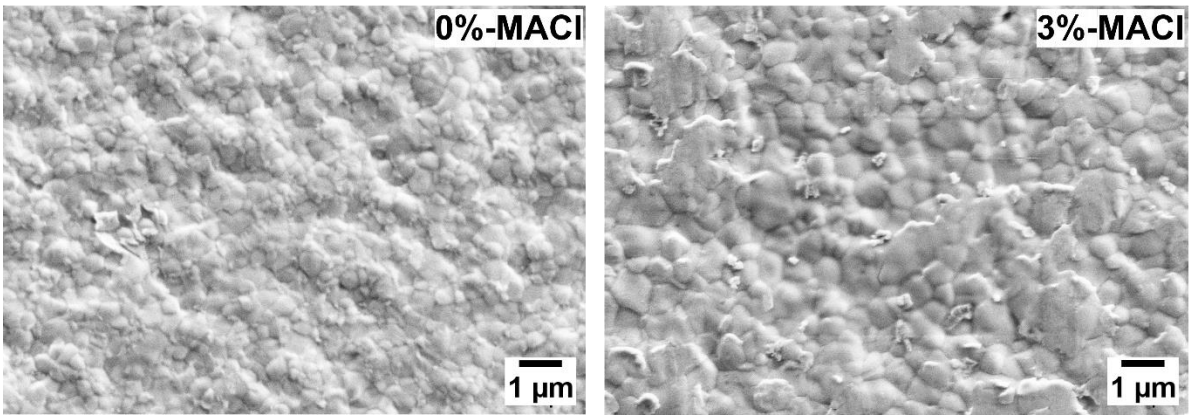

Figure S5. SEM images presenting vanished pinholes after annealing for 7 min for the perovskite films with and without MACl.

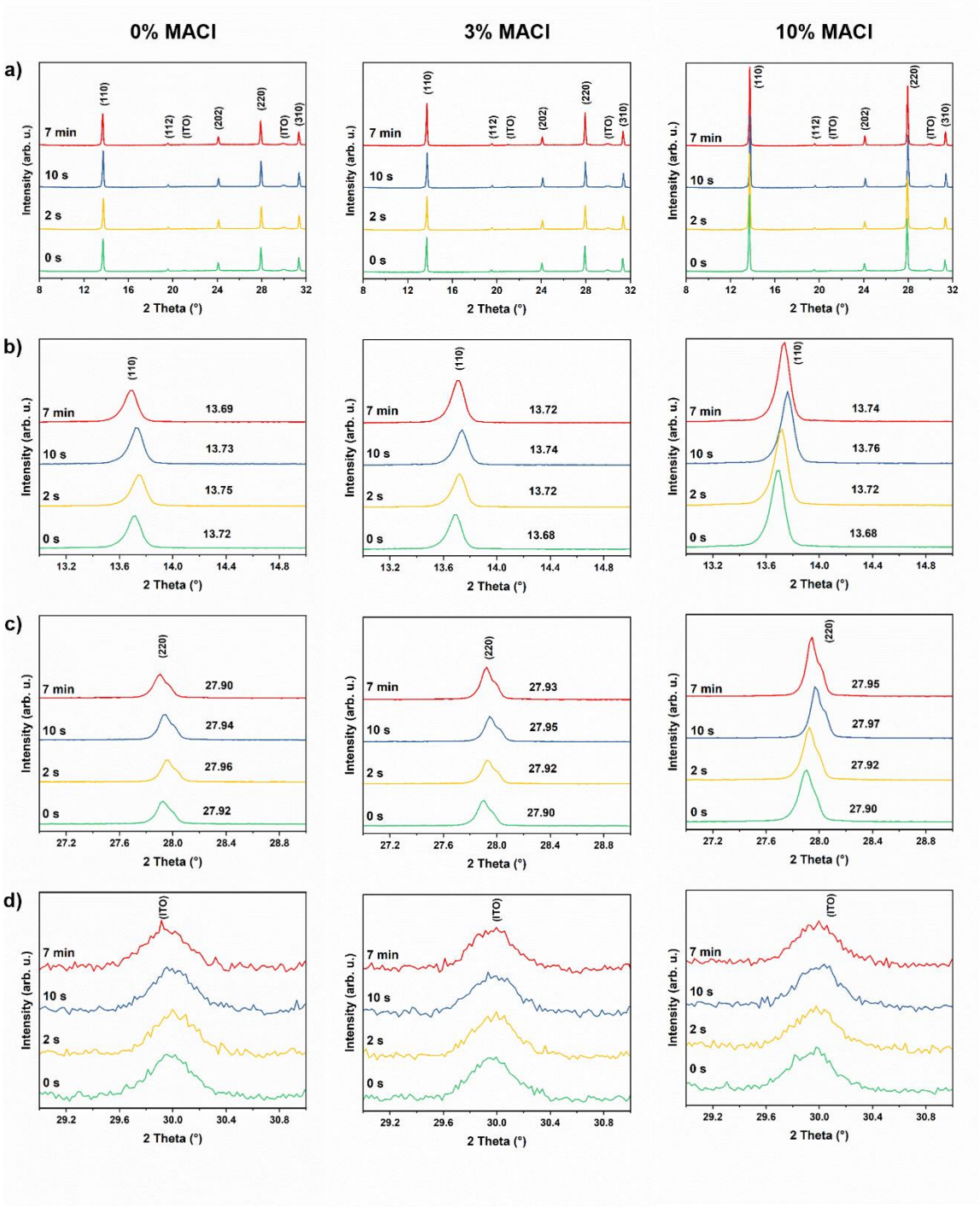

Figure S6. (a) XRD patterns and zoom-in planes of (b) (110), (c) (220), and (d) ITO for the perovskite films with varied concentrations of MACl before annealing (0 s), and after annealing for 2 s, 10 s, and 7 min.

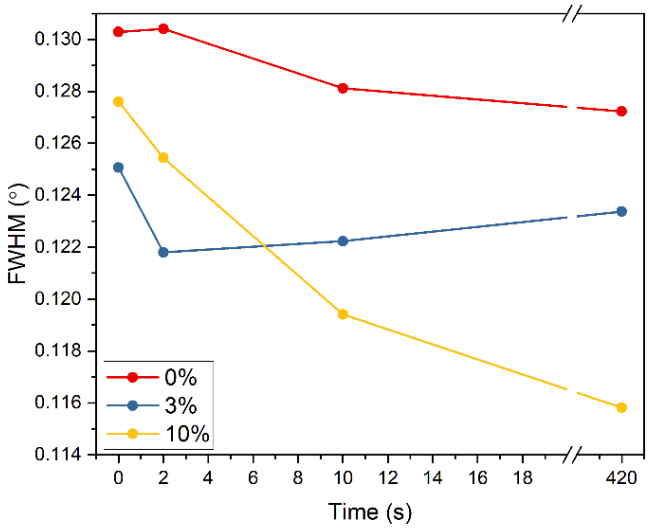

Figure S7. The full width at half maximum (FWHM) of the diffraction (110) plane for the perovskite films with varied concentrations of MACl before annealing (0 s), and after annealing for 2 s, 10 s, and 7 min.

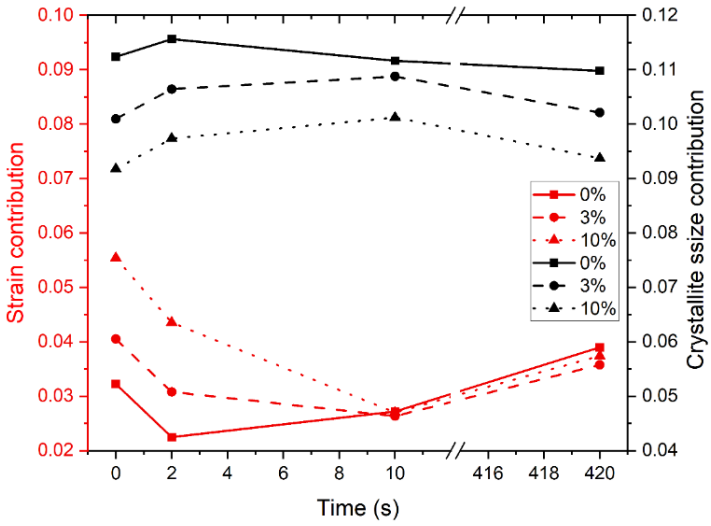

Figure S8. Strain evolution for the perovskite films with varied concentrations of MACl before annealing (0 s), and after annealing for 2 s, 10 s, and 7 min.

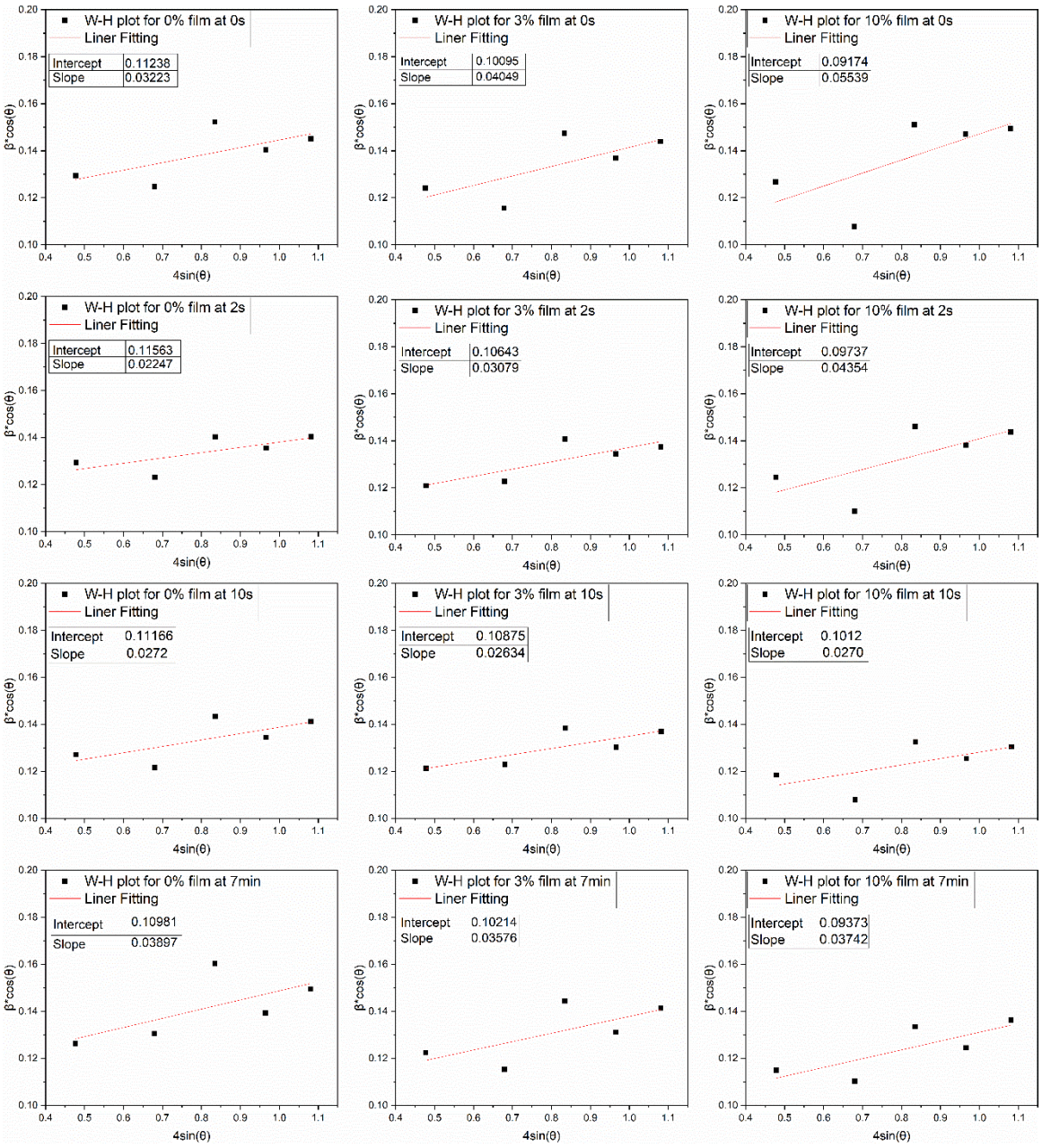

Figure S9. Williamson-Hall analysis for the perovskite films with varied concentrations of MACl before annealing (0 s), and after annealing for 2 s, 10 s, and 7 min.

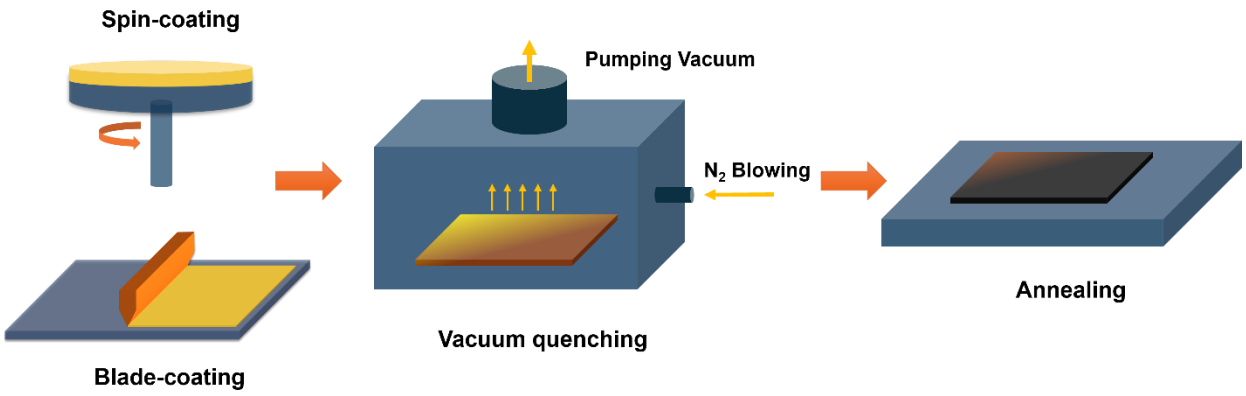

Figure S10. Schematic illustration of fabrication process of spin-coated (SC) and blade-coated (BC) perovskite thin films.

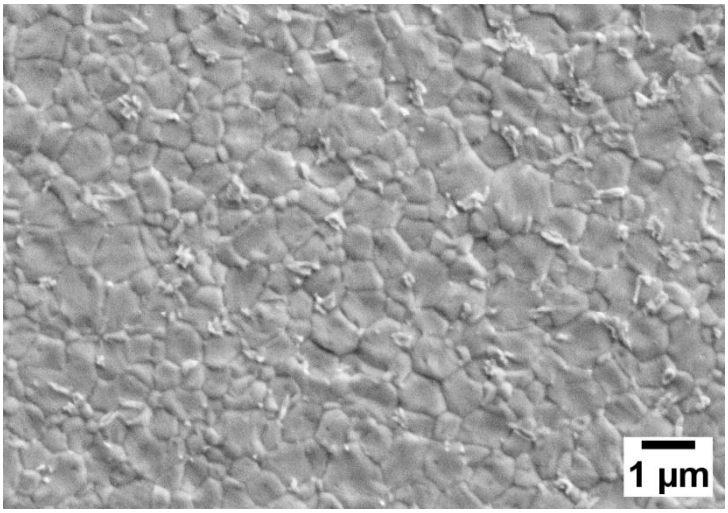

Figure S11. SEM images of NBG perovskite film with antisolvent method.

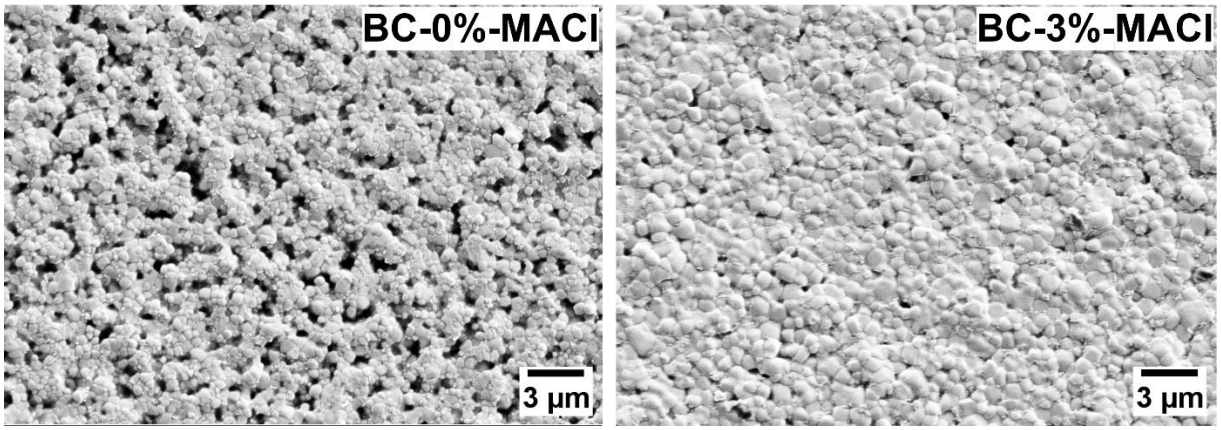

Figure S12. SEM images of blade-coated (BC) perovskite thin films with and without MACl.

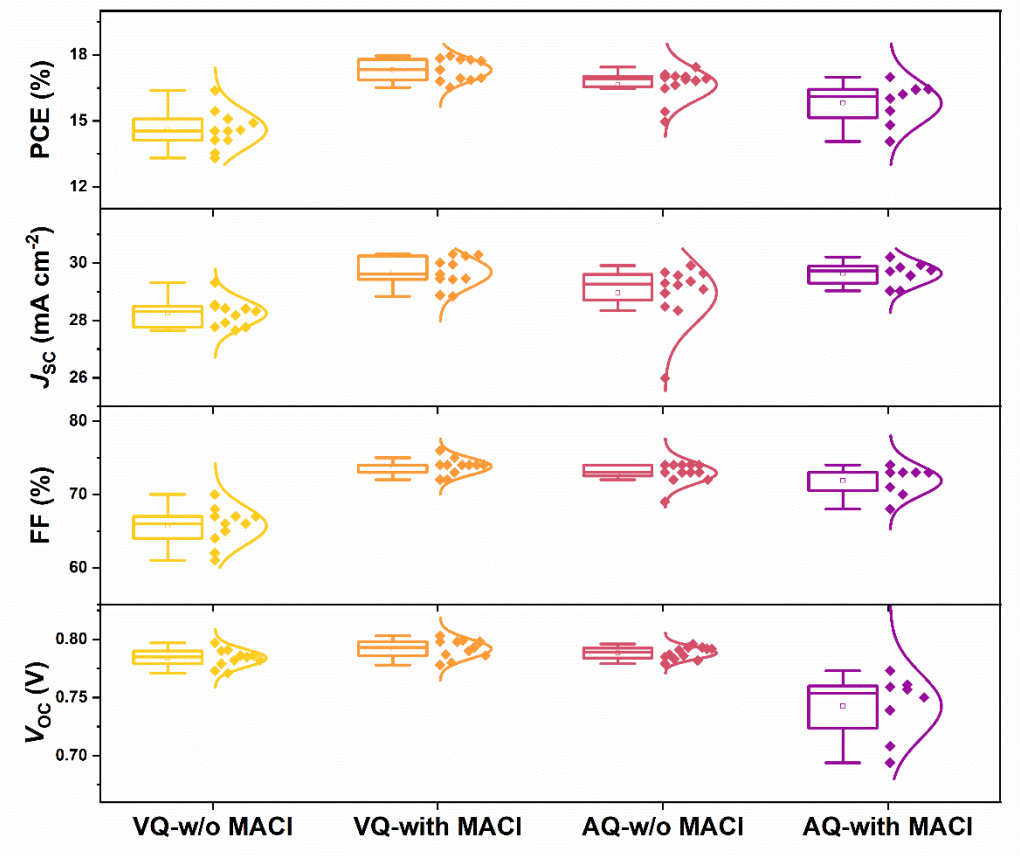

Figure S13. Statistical distribution of the photovoltaic parameters of SC-NBG PSCs fabricated by using vacuum quenching (VQ) and anti-solvent quenching (AQ) methods with and without MACl.

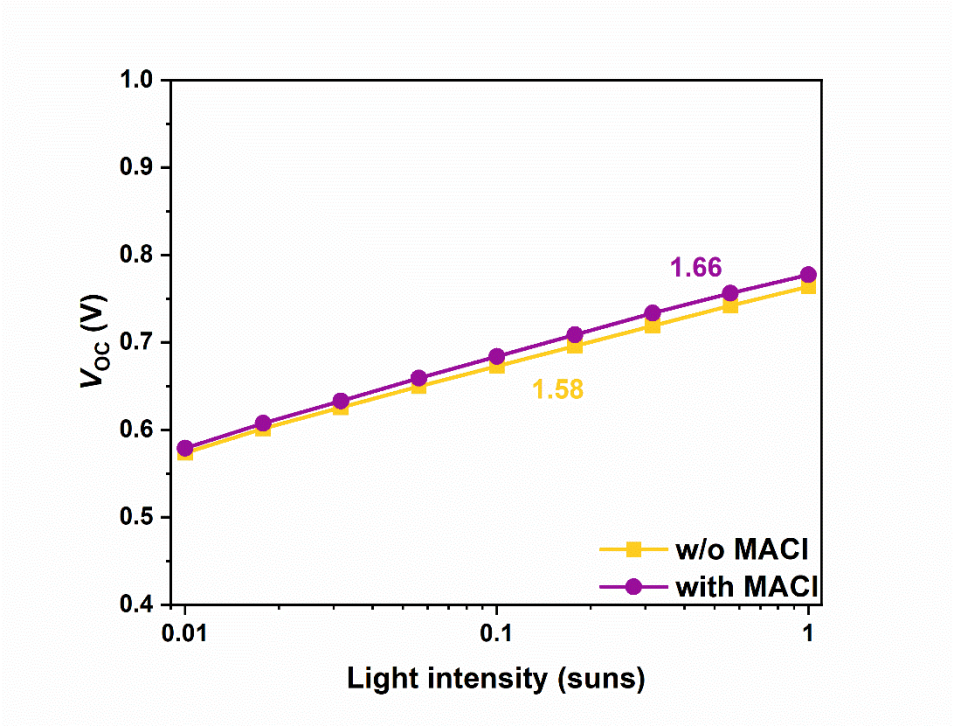

Figure S14. Illumination intensity-dependent V_{OC} of the PSCs with and without MACl.

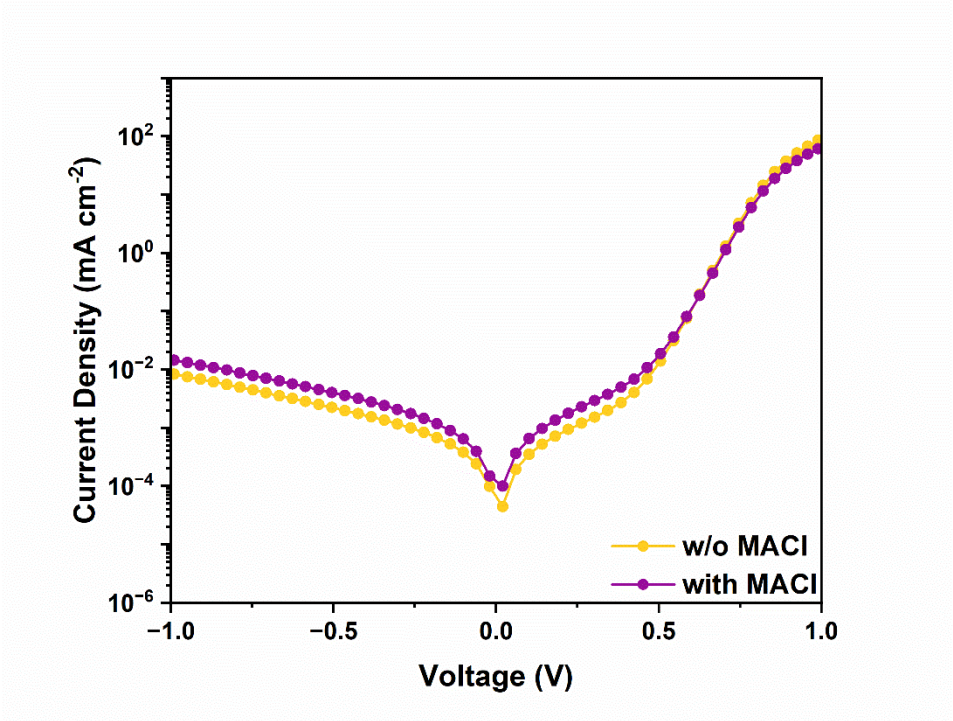

Figure S15. Dark *J-V* curves of the PSCs with and without MACl.

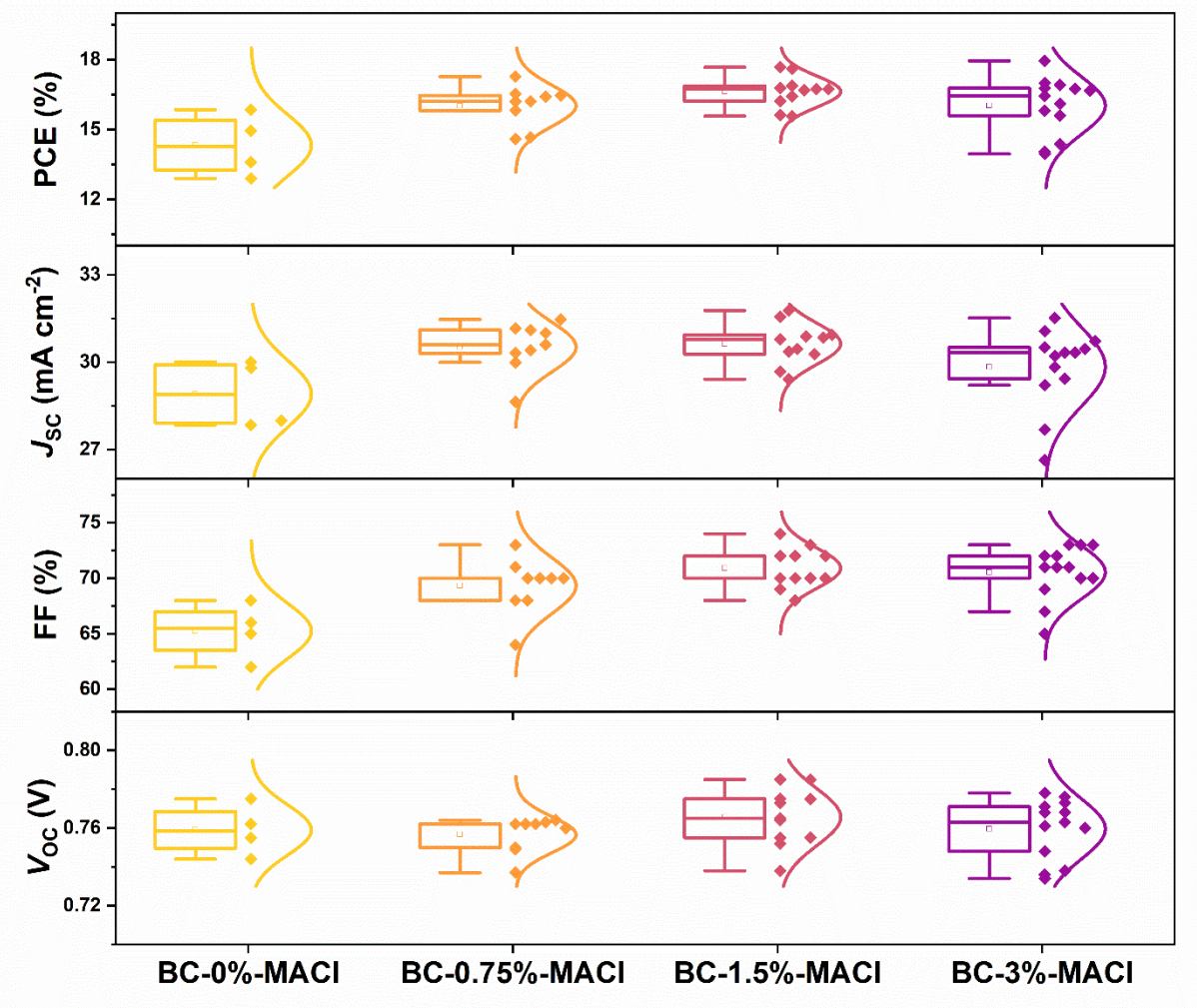

Figure S16. Statistical distribution of the photovoltaic parameters of BC NBG PSCs with varied MACl concentrations.

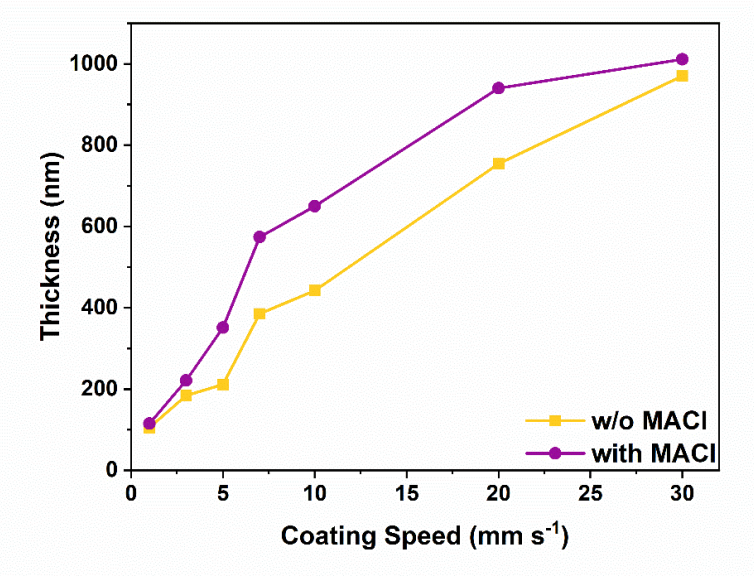

Figure S17. Thickness variation of blade-coated perovskite films with or without MACl additive under different coating speed.

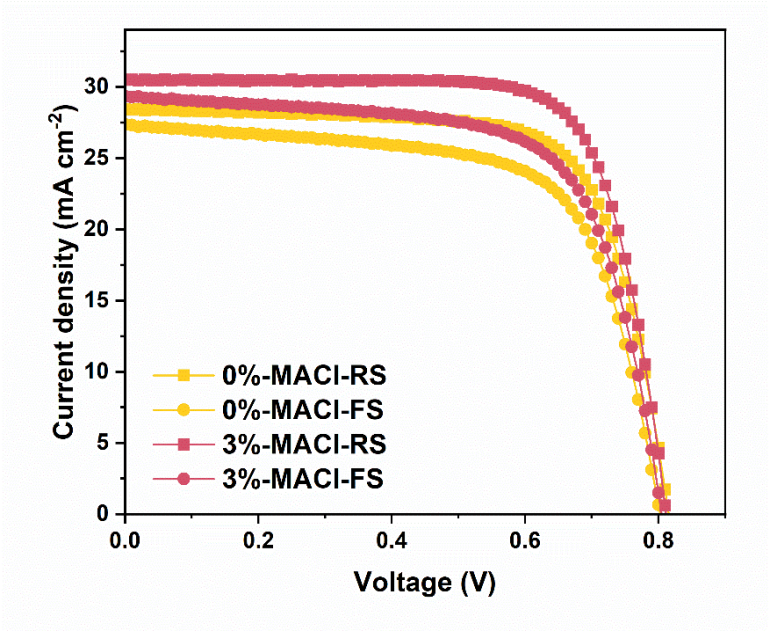

Figure S18. Forward and reverse *JV* scans of the SC NBG solar cells with 0% and 3% MACl addition. Scan parameters for both direction: scan rate: 0.6 V s^{-1}; step size: 10 mV; no preconditioning.

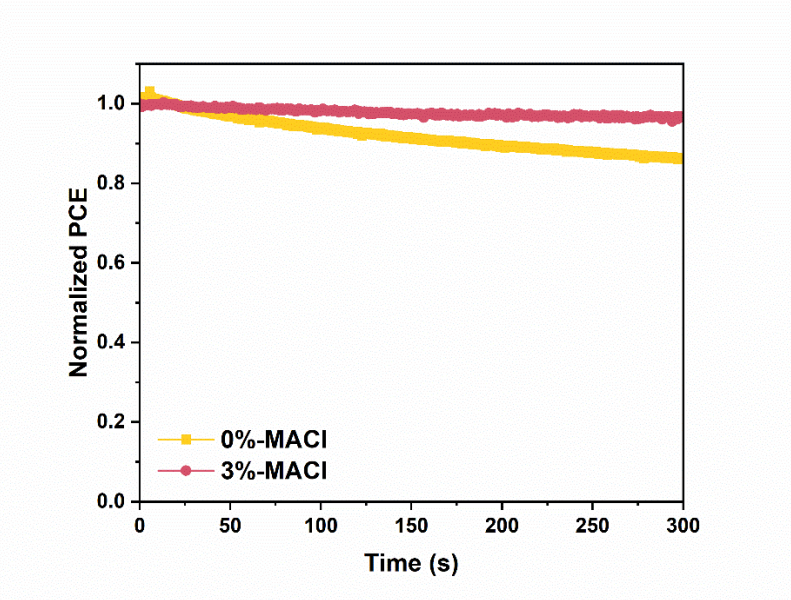

Figure S19. Maximum power point (MPP) tracking of the SC NBG solar cells with 0% and 3% MACl addition.

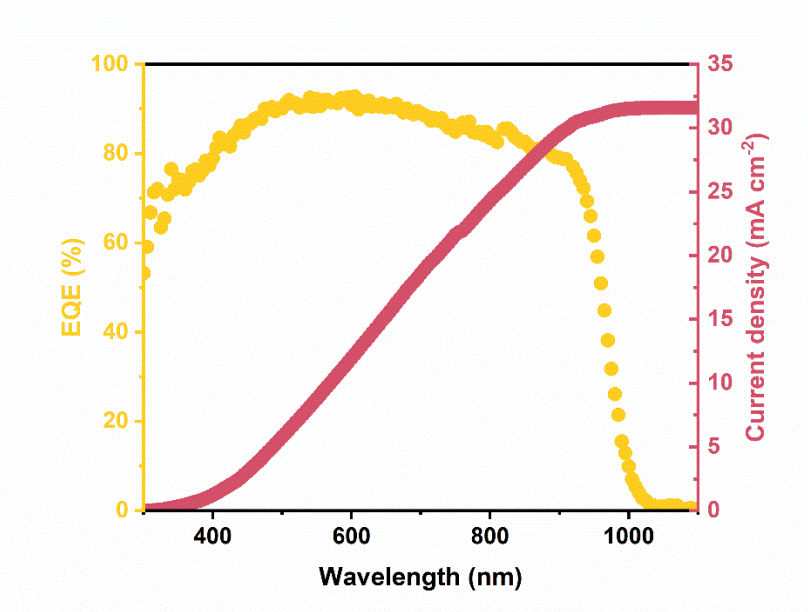

Figure S20. The external quantum efficiency (EQE) spectrum of the SC NBG PSCs with MACl with an integrated J_{SC} of 31.6 mA cm^{-2}.

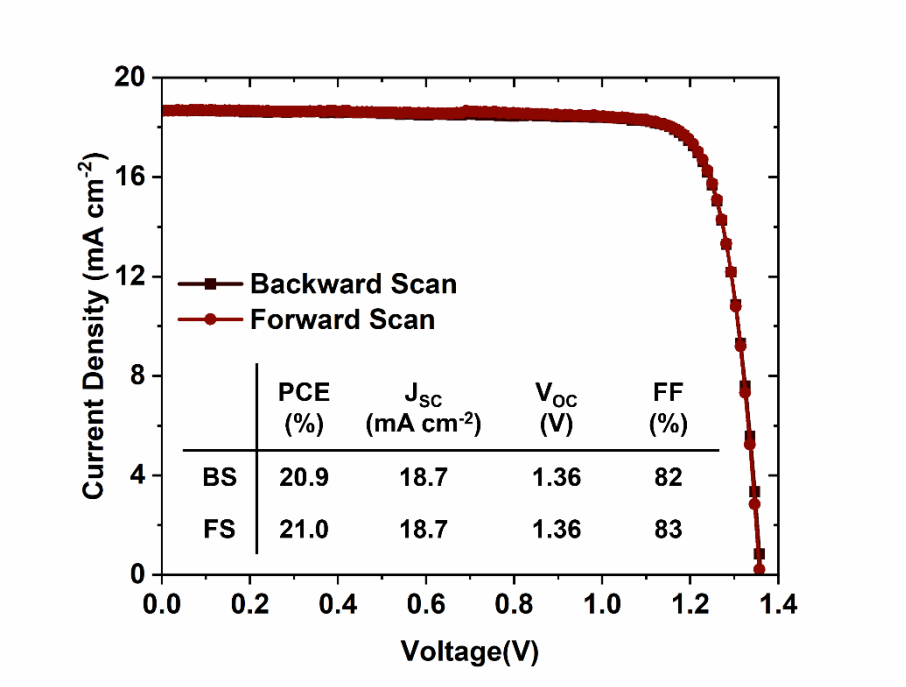

Figure S21. *J-V* curves (forward and backward scans) of the champion wide-bandgap (WBG) perovskite solar cell under continuous AM 1.5G illumination.